NEW VIEWS ON FAULTING, FABRIC DEVELOPMENT, AND VOLUME STRAIN IN THE TACONIC SLATE BELT, WESTERN VERMONT AND EASTERN NEW YORK

by
Jean M. Crespi, Jonathan R. Gourley, and Christine M. Witkowski, Department of Geology and Geophysics, University of Connecticut, Storrs, CT 06269

INTRODUCTION

Slate belts provide an important window into tectonic processes, because they preserve bedding despite the penetrative character of the deformational fabric. The reference frame given by bedding, together with information from strain markers, permits quantitative understanding of the deformation since deposition of the strata. Although the complete deformational history can rarely, if ever, be determined, approaches that involve the integration of different types of data are more likely to advance understanding.

The northernmost part of the Taconic Allochthon (Fig. 1) in western Vermont and eastern New York is one of the best studied slate belts in the world. Geological studies (Dale, 1899) accompanied the development of the quarrying industry, which began in the area in the 19th century, and the Taconic orogenic belt was one of the first ancient orogenic belts to be interpreted in the context of plate tectonics (Chapple, 1973). An arc-continent collision interpretation still stands for the origin of the orogenic belt (Chapple, 1973; Rowley and Kidd, 1981; Stanley and Ratcliffe, 1985); however, debate centers on whether the colliding volcanic arc was the Bronson Hill arc or the more inboard and older Shelburne Falls arc (Karabinos et al., 1998, 1999; Ratcliffe et al., 1998, 1999). Geochronologic and biostratigraphic data (Zen, 1967; Laird et al., 1984; Sutter et al., 1985; Ratcliffe et al., 1998) indicate that collisional orogenesis occurred during Middle to Late Ordovician time. The Taconic Allochthon formed as Cambrian?/Cambrian to Middle Ordovician slope and rise strata were thrust west onto approximately coeval strata of the carbonate platform.

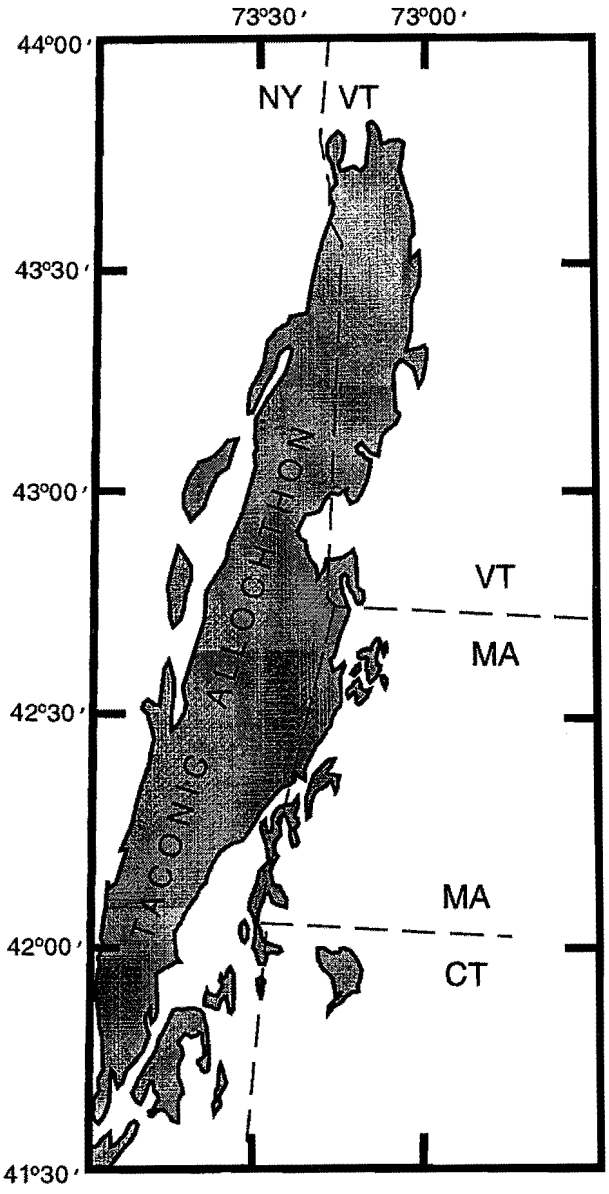

Figure 1. Index map to Taconic Allochthon.

The strata within the slate belt of the northernmost Taconic Allochthon were deformed into a series of west-vergent, tight to isoclinal folds during the main phase (D_2) of deformation. The slaty cleavage (S_2) is parallel or lies at a very low angle to the axial planes of the F_2 folds. Although Zen (1961) proposed that the slate belt is characterized by recumbent and downward-facing folds, implying an earlier D_1 phase of deformation, Bosworth and Rowley (1984) showed that F_1 folds are relatively rare. Locally, S_2 is overprinted by a weakly to moderately developed crenulation cleavage (S_3). Recently obtained $^{40}Ar/^{39}Ar$ ages from closely packed S_3 domains are Devonian and are interpreted as consistent with Acadian rather than Taconian orogenesis (Chan et al., 2001).

This field trip guide builds on a previous NEIGC guide to the area (Goldstein et al., 1997): several outcrops from the 1997 trip are reexamined on this trip in light of

new data from a variety of strain markers. In particular, we compare results from markers that record the total strain with those from markers that record different portions of the total strain. Aspects of the deformation that we focus on include evidence for prelithification tectonic deformation; volume change associated with S_2 development; and variations in S_2 orientation and state of strain with structural level. We also present new observations of meso- and microscale structures within the Bird Mountain slice. Specifically, we focus on the information that these structures provide on the movement history of the Bird Mountain fault with respect to regional deformational events.

STRAIN MARKERS: PREVIOUS AND CURRENT WORK

Strain markers have been analyzed in three stratigraphic units in the Taconic slate belt (Fig. 2). Black slates of the Cambrian Hatch Hill Formation and Ordovician Mount Merino Formation contain strain fringes around pyrite framboids and graptolites. Analyses of strain fringes in the Hatch Hill Formation are presented in Chan (1998); current research focuses on those in the Mount Merino Formation. Because graptolites are not abundant in the Hatch Hill Formation, strain analyses have been conducted only on those in the Mount Merino Formation. Goldstein et al. (1998) used thecal spacing measurements to extract strain values from the graptolites. Two alternative approaches are the subject of current research: reconstruction of the fractured and displaced pyrite blocks forming the graptolites and determination of the surface separating the extension and shortening fields of the instantaneous strain ellipsoid. Finally, maroon slate of the Cambrian Mettawee Formation contains reduction spots. These have been studied by Wood (1974), Hoak (1992), and Goldstein et al. (1995).

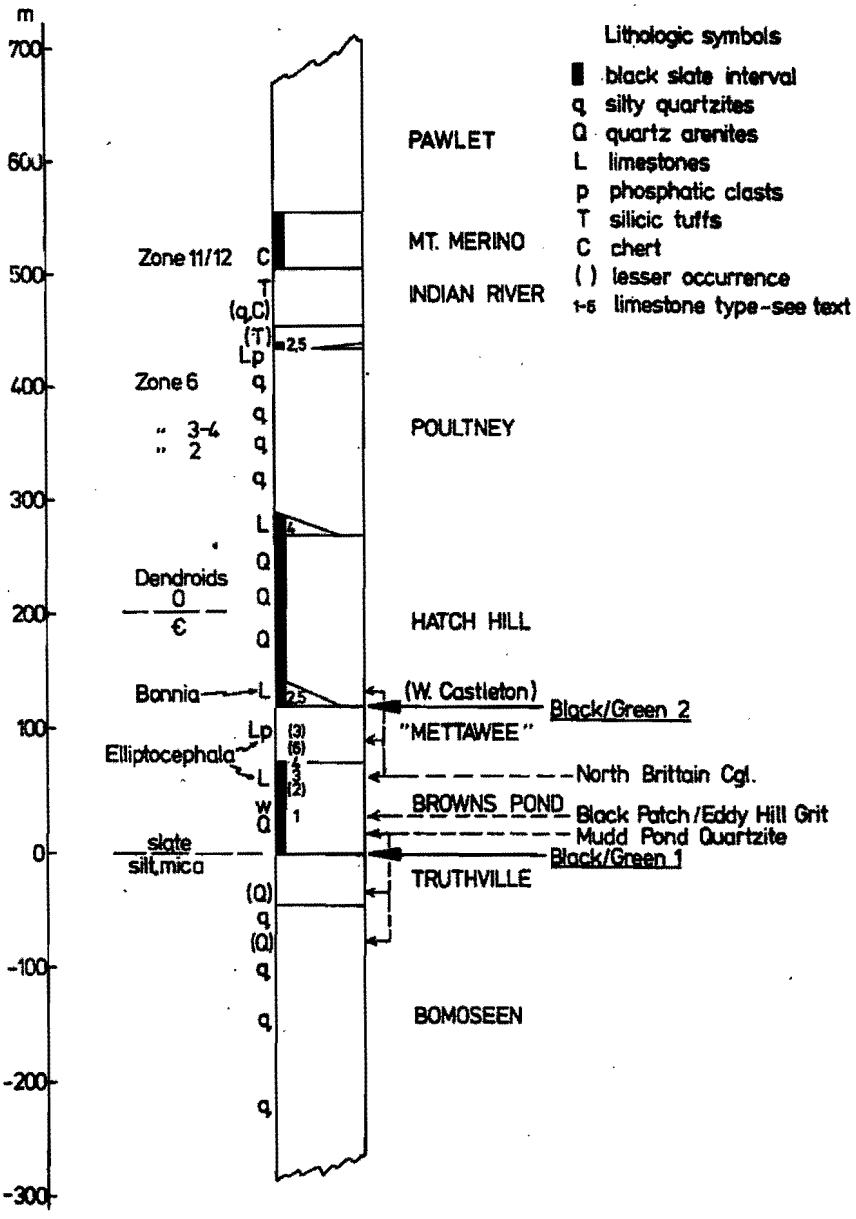

Figure 2. Stratigraphy of Taconic sequence (from Rowley et al. (1979)).

Strain Fringes

Chan (1998) analyzed strain fringes around pyrite framboids in the Hatch Hill Formation along a transect in the vicinity of Route 4 (Fig. 3). The strain fringes are composed of quartz and phyllosilicate fibers, and fiber growth is inferred to be antitaxial on the basis of the marked compositional difference between

the fibers and core object. Along the transect, S_2 dips about 30° to the east, and the mineral lineation (L_2) plunges to the east-southeast. Strain fringes were sampled from four upright and one overturned regional-scale F_2 fold limbs.

In S_2-parallel thin sections (*XY* sections; *X*>=*Y*>=*Z*), the strain fringes indicate plane-strain deformation: the fibers are straight and parallel to L_2, and the strain fringes, which completely bracket the pyrite framboid, do not change width with distance from the framboid. In thin sections cut perpendicular to S_2 and parallel to L_2 (*XZ* sections), the fibers are curved and the sense of curvature is consistent along the transect. Viewed to the north-northeast, individual fibers curve counterclockwise when traced from the portion closest to the framboid to the portion furthest from the framboid, i.e., from youngest to oldest increments of fiber growth. In addition, the youngest increment of fiber growth, which is inferred to lie parallel to the maximum instantaneous stretching axis, is oriented at an angle to S_2. Chan (1998) used these and several other characteristics to infer that fiber growth occurred only during S_2 development and that S_2 development was within a zone of top-to-west-northwest, non-coaxial flow.

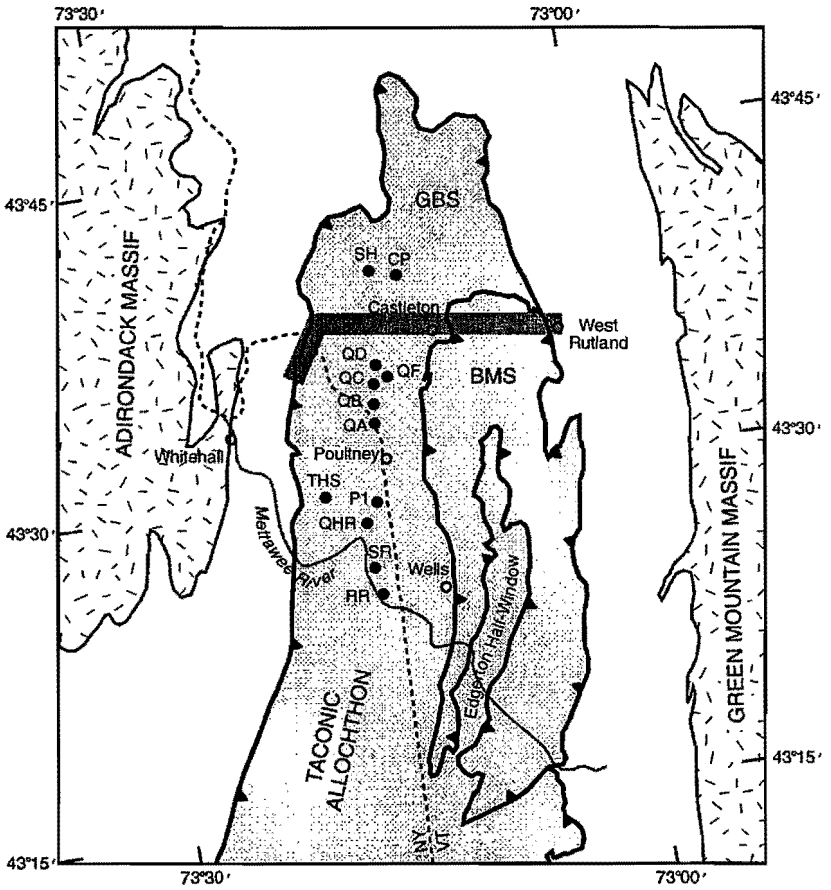

Figure 3. Simplified geological map of northern Taconic Allochthon and surrounding region. GBS--Giddings Brook slice; BMS--Bird Mountain slice; CP, SH, QA, QB, QC, QD, and QF--reduction spot sites from Wood (1974), Hoak (1992), and Goldstein et al. (1995); SR, P1, QHR, RR, and THS--graptolite sites from Goldstein et al. (1998); thick gray line--transect from Chan (1998); unpatterned area--carbonate platform.

Because no strain analysis technique for strain fringes has been designed specifically for fibers that form during non-coaxial flow, Chan (1998) applied the Durney and Ramsay (1973) technique to strain fringes in *XZ* thin sections to make comparisons along the transect of fiber shape and length. Both are relatively uniform. In particular, the mean maximum principal finite stretch ($1 + e_1$) calculated from the fibers using the Durney and Ramsay (1973) technique ranges only between 2.1 and 2.4 for the sites. Chan (1998) used this result as well as the nearly constant orientation of S_2 to infer that the transect lies along the same structural level within a regional-scale shear zone that formed in the pressure-solution regime.

Strain fringes around subspherical core objects in the Mount Merino Formation have been analyzed at three sites around a regional-scale F_2 fold (Fig. 3): on the overturned limb where S_0 and S_2 are essentially parallel (site SR1); on the upright limb where S_0 and S_2 lie at a moderate angle (site SR3); and in the hinge zone where S_0 and S_2 are perpendicular or nearly so (site SR5). Site names are after Goldstein et al. (1998). The sites lie about twenty kilometers south of the transect studied by Chan (1998). S_2 shows little variation in orientation between the three sites and dips about 45°-50° to the east.

The subspherical core objects hosting the strain fringes are framboidal pyrite or a hydrous mineral that replaced the pyrite as evidenced by a discontinuous rim of pyrite at the replaced core-object/fringe interface. The strain fringes are composed of quartz and phyllosilicate fibers, and fiber growth is inferred to be antitaxial. In *XY* thin sections, the strain fringes completely surround the core objects, and the fibers display approximately radial growth. These characteristics imply flattening strain such that extension occurred in all directions in the S_2 plane. The mean orientation of the longest dimension of the strain fringes at a site is taken as a proxy for L_2, which is difficult to identify in the hand samples. L_2 may not be well expressed because of the flattening character of the strain, the relatively low magnitude of the S_2-related strain, and the presence of a well-developed, S_0-parallel phyllosilicate fabric. The mean orientations of the longest dimension of the strain fringes plunge to the southeast. In *XZ* thin sections, the fibers within the strain fringes display one of two geometries. In one type, the fibers are essentially straight but lie at a low angle to the trace of S_2. In the other type, the fibers are very gently curved and lie generally parallel to the trace of S_2. These characteristics are interpreted as reflecting non-coaxial flow, and the asymmetries of the two types of strain fringes are consistent with top-to-northwest sense of shear.

Quantification of the strain recorded by the strain fringes in the Mount Merino Formation is complicated not only by the fringes having formed during non-coaxial flow but also by a cut-effect problem resulting from the flattening nature of the strain. Because the core objects are not necessarily intersected in their centers, measurements in *XZ* thin sections will overestimate the strain. Extension values, therefore, were determined in *XY* thin sections. Measurements were made along the longest and shortest dimensions of the strain fringes through the center of the core objects, using the length of the core object as l_o and the total length of the fringes and core object as l_f. This results in minimum estimates of strain magnitude because of the non-coaxiality of the flow and because pressure solution locally occurred along the margins of the strain fringes as seen in *XZ* thin sections. The former reason is probably not significant, because the small amount of fiber curvature suggests low degrees of non-coaxiality. For the three sites, mean values for $1 + e_1$ range from 1.5 to 1.65, and mean values for $1 + e_2$ range from 1.15 to 1.3.

Graptolites

Three species of graptolites in the Mount Merino Formation were used by Goldstein et al. (1998) to estimate strain: *Orthograptus whitfieldi*, *Orthograptus calcaratus*, and *Climacograptus bicornis*. In the undeformed state, the spacing between thecae is constant for these species, with the exception of the first few thecae added to the stipe. Absolute changes in length on the S_0 plane, therefore, can be determined through measurements of the deformed thecal spacing. Goldstein et al. (1998) accomplished this for eight sites in the Mount Merino Formation (Fig. 3). The undeformed thecal spacing for each of the three species was determined from graptolite-bearing shales deposited in close proximity, both with respect to space and time, to the Mount Merino Formation.

Because the F_2 folds in the Taconic slate belt are tight to isoclinal, Goldstein et al. (1998) were able to determine the lengths of the principal axes of the finite strain ellipsoid despite the restriction that thecal spacing measurements allow strain determination only for the S_0 plane. Values for $1 + e_1$ and $1 + e_2$ were estimated from samples obtained from the limbs of folds where S_0 and S_2 are essentially parallel, and values for $1 + e_3$ were estimated from samples from the hinge zone of a fold. By assuming homogeneous strain across the folds, Goldstein et al. (1998) combined limb and hinge data to calculate the volume change undergone by the strata. The volume change values obtained from the data set range from a volume gain of 7% to a volume loss of 81%; the average is a volume loss of 53%. For the SR sites, which are the subject of current research, the volume change values range from losses of 68% to 81%. Goldstein et al. (1998) inferred that the volume loss occurred during the development of S_2.

Graptolites from the SR sites were analyzed in more detail, because the sites lie at different structural positions, including the hinge zone, around a single fold (see above). Moreover, graptolite-bearing strata of the Mount Merino Formation are not exposed in the hinge zone of any other fold in the Taconic slate belt. Microstructural observations show that the graptolite periderms have been replaced by pyrite and that deformation of the graptolites has been accommodated by fracturing of the pyrite into blocks and displacement of the pyrite blocks relative to each other. Fractures across which blocks have separated are filled with fibrous chlorite. Fibrous chlorite also typically forms strain fringes along the margins of the graptolites at the pyrite-matrix interface.

In *XY* thin sections from site SR1 (Fig. 4a), where S_0 and S_2 are essentially parallel, chlorite-filled fractures generally form two sets, one approximately normal to the *X*-axis and the other approximately normal to the *Y*-axis. This orthogonal fracture system shows that graptolites subparallel to S_2 have undergone chocolate tablet boudinage. In *XY* thin sections from site SR5 (Fig. 4b), where S_0 and S_2 are at an angle to each other, graptolites lie along the S_0-S_2 intersection lineation. These graptolites are cut by a single set of fractures, which has allowed the graptolites to extend parallel to the intersection lineation. Extension at a high angle to the graptolites is expressed as chlorite strain fringes along the pyrite-matrix interface. Graptolites have not been examined in *XY* thin sections from site SR3.

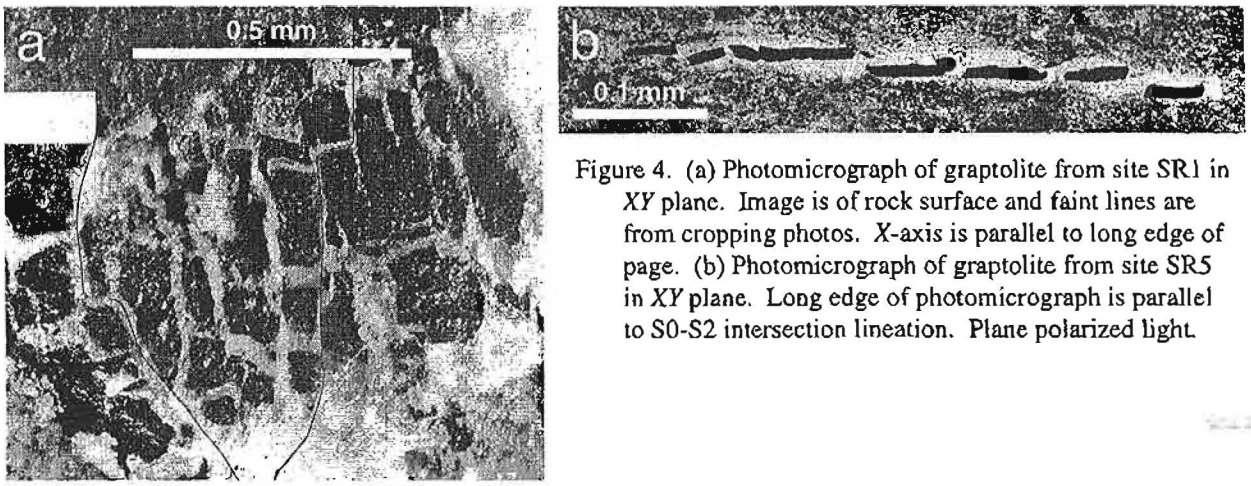

Figure 4. (a) Photomicrograph of graptolite from site SR1 in *XY* plane. Image is of rock surface and faint lines are from cropping photos. *X*-axis is parallel to long edge of page. (b) Photomicrograph of graptolite from site SR5 in *XY* plane. Long edge of photomicrograph is parallel to S0-S2 intersection lineation. Plane polarized light.

In *XZ* thin sections from site SR1 (Fig. 5a), the fractures may be oblique to the graptolites and have a component of fracture-parallel displacement, but they more commonly are normal to the graptolites. Graptolites in *XZ* thin sections from site SR5 (Fig. 5b) lie at a high angle to S_2 and have undergone shortening by rotation and imbrication of the pyrite blocks to effectively fold the graptolites. Graptolites in *XZ* thin sections from site SR3 (Fig. 5c) lie at a moderate angle to S_2. These graptolites show evidence of both shortening and extension: shortening is expressed by imbricated pyrite blocks, and extension by pyrite blocks that were once joined but are now separated by a chlorite-filled fracture.

Preliminary measurements of the change in length undergone by the graptolites have been made by restoring the displaced pyrite blocks to their inferred original positions. Because the graptolites are viewed in two dimensions, i.e., either in *XY* or *XZ* thin sections, but have deformed in three dimensions, restorations, in some cases, require compensation for cut-effect problems. In particular, chlorite-filled fractures accommodating extension normal to the thin section must be distinguished from those accommodating extension in the plane of the thin section. Where this cannot be done successfully using fine details of pyrite block morphology, maximum and minimum values for the change in length are determined. Three observations suggest that the measured changes in length are reasonable approximations for the strain undergone by the matrix. First, there is no evidence that the pyrite has undergone pressure solution. Second, pyrite does not appear to deform internally during greenschist facies metamorphism. Finally, strain shadows are not noticeable adjacent to shortened graptolites, and S_2 does not wrap around or only very slightly wraps around shortened graptolites. This implies little competency contrast between the graptolites and surrounding matrix, which may be a result of the very high aspect ratio of the graptolites.

Preliminary results obtained from the pyrite block restorations are as follows. Average values for $1 + e_1$ and $1 + e_2$ determined from site SR1 are 1.35 and 1.2, respectively. The average value for $1 + e$ in the direction of the S_0-S_2 intersection lineation determined from site SR5 is 1.15. $1 + e_2$ can be calculated from this result using the $1 + e_1$ value from site SR1 and equation (3-31) of Ramsay (1967). This gives a value of 1.1 for $1 + e_2$, which when averaged with the value for $1 + e_2$ from site SR1, gives an average $1 + e_2$ of 1.15. The minimum and maximum average values for $1 + e$ along S_0 in the *XZ* plane for site SR3 are 0.9 and 1.1. $1 + e_3$ can be calculated using the

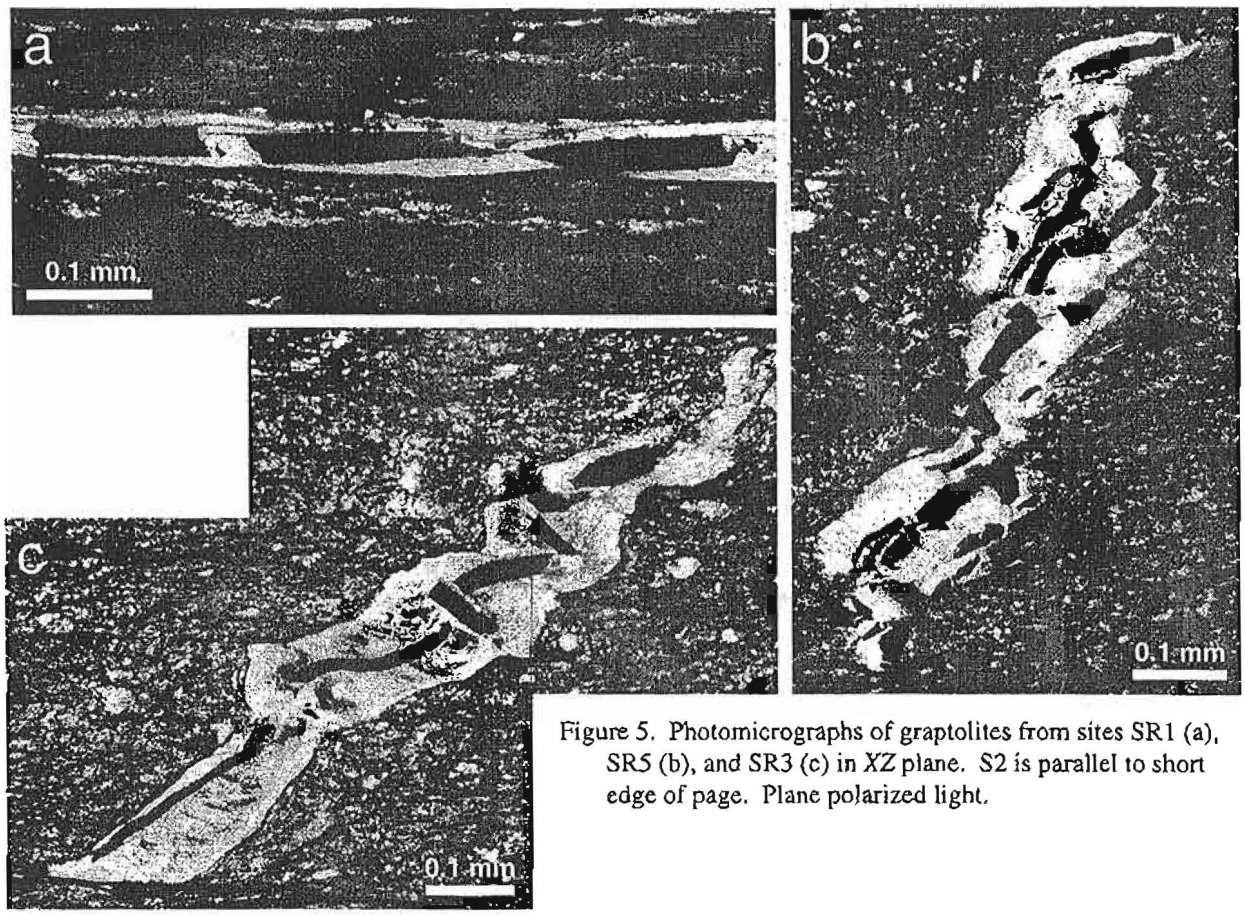

Figure 5. Photomicrographs of graptolites from sites SR1 (a), SR5 (b), and SR3 (c) in *XZ* plane. S2 is parallel to short edge of page. Plane polarized light.

$1 + e_1$ value from site SR1, the $1 + e$ values from site SR3, and equation (3-31) of Ramsay (1967); calculated minimum and maximum values for $1 + e_3$ are 0.65 and 0.85.

Reduction Spots

Reduction spots, which are inferred to form early during diagenesis, record the total strain undergone by the strata, including burial compaction or some portion thereof. In aggregate, reduction spots have been analyzed at nine sites in the Mettawee Formation (Fig. 3). Wood (1974), Hoak (1992), and Goldstein et al. (1995) acquired data from six, four, and seven sites, respectively, but a number of sites overlap between the different studies. As noted by Goldstein et al. (1995), the results obtained by different workers from the same site are similar.

There is a large amount of scatter in the shape of the reduction spots, and this variation exists on the scale of individual blocks, between blocks from the same site, and between sites (Goldstein et al., 1995). The shape variation of the reduction spots results primarily from large variation in *YZ* axial ratio and small variation in *XY* axial ratio (Goldstein et al., 1995). In all cases, the short axes of the reduction spots lie perpendicular to S_2. Because several workers have measured reduction spots in the Mettawee Formation and the measurement technique obviates duplication of the same reduction spot, the Flinn diagram shown in Fig. 6 plots weighted means for each site using data from Wood (1974), Hoak (1992), and Goldstein et al. (1995). The weighting is based on the number of reduction spots measured by each worker at a given site, and only sites measured by more than one worker are included. Like the data presented in Goldstein et al. (1995), these data lie in the field of apparent flattening and define an essentially horizontal line on a Flinn diagram.

Wood (1974) used the reduction spot data to illustrate how a deformation path can be determined from spatial heterogeneities in finite strain. Goldstein et al. (1995) followed up on this concept to estimate the volume change undergone by the Mettawee Formation during S_2 development. They argued that, because the strata in all likelihood underwent plane-strain deformation during S_2 development, the lack of variation in *XY* axial ratio implies shortening along the *Z*-axis without compensating extension along the *X*-axis. This necessitates a loss in volume. By comparing data from the least and most strained sites, Goldstein et al. (1995) estimated a minimum volume loss during S_2 development of 55%.

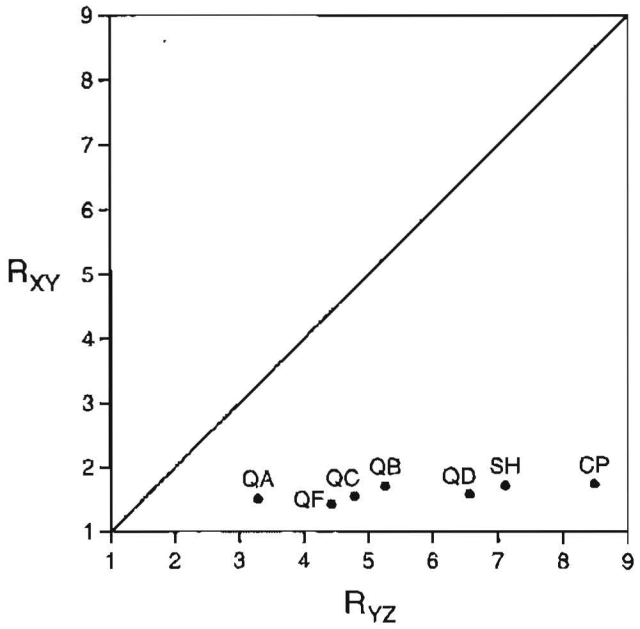

Figure 6. Flinn diagram of average shapes of reduction spots in Mettawee Formation. Data compiled from studies by Wood (1974), Hoak (1992), and Goldstein et al. (1995). Site names from Goldstein et al. (1995). QA, QB, QC, QF, and SH are limb sites; QD and CP are hinge sites.

STRAIN MARKERS: INTERPRETATION

Integration of the results obtained from the different strain markers suggests several revisions in our understanding of the structural development of the Taconic slate belt. The interpretations, in some cases, are preliminary and are likely to evolve with the acquisition of more data.

Strain Fringes

Strain fringes around subspherical core objects from the transect in the vicinity of Route 4 and from the SR sites display characteristics consistent with formation during foreland-directed, non-coaxial flow. On the basis of these and other observations, the fringes are inferred to have formed at the same time as S_2 in a regional-scale shear zone that formed in the pressure-solution regime. The strain fringes from the two areas, however, differ in three fundamental ways. First, fringes from the transect in the vicinity of Route 4 record plane-strain deformation, whereas those from the SR sites record flattening strain. Second, fringes from the transect in the vicinity of Route 4 yield higher values for $1 + e_1$ than those from the SR sites. Third, fibers within strain fringes from the transect in the vicinity of Route 4 display higher degrees of curvature than those in fringes from the SR sites. These differences, together with the contrast in dip of S_2 in the two areas, suggest exposure of different structural levels of the inferred shear zone.

Theoretical models show that foliation orientation changes within a shear zone as a result of variations in the amount of strain and/or the degree of non-coaxiality (Ramsay and Graham, 1970; Sanderson, 1982). In the case of end-member simple shearing, for example, the angle between foliation and the shear plane decreases with increasing strain magnitude from 45° for incipient foliation development to nearly 0° for very high strains. The angle between foliation and the shear plane also decreases systematically with increasing strain magnitude in zones of general flow, i.e., non-coaxial flow other than simple shearing, the exact angular relations depending upon the degree of non-coaxiality and whether the shear zone is a thickening or thinning shear zone (Weijermars, 1991). It follows that spatial variations in the degree of non-coaxiality within a shear zone can produce changes in foliation orientation regardless of variations in strain magnitude.

Regional cross sections (Ando et al., 1984) show that the base of the Taconic Allochthon is a very low dipping surface. Although this surface is mapped as a post-S_2 thrust fault (Bosworth and Rowley, 1984), it is probably approximately parallel to the shear plane for the shear zone in which S_2 developed. The SR sites are inferred to lie at a relatively high structural level within the shear zone and the transect in the vicinity of Route 4 is inferred to lie at a relatively low structural level on the basis of the higher S_2 dip and lower $1 + e_1$ value for the SR sites. The

difference in degree of fiber curvature between the SR sites and the transect in the vicinity of Route 4 suggests that the degree of non-coaxiality may be less at relatively high structural levels within the shear zone, although this is difficult to quantify. The presence of flattening as opposed to plane strain at the SR sites implies a change in boundary conditions with structural level.

This interpretation of the Taconic slate belt in the context of structural levels is consistent with regional structural and stratigraphic relations. The Taconic Allochthon and underlying autochthonous strata of the carbonate platform are gently folded to form the Middlebury synclinorium. The synclinorium plunges gently to the south (Zen, 1967), as implied by the northern closure of the Taconic Allochthon. This results in the exposure of systematically shallower structural levels from north to south within the Allochthon. In addition, units higher in the Taconic sequence are more common at Earth's surface in the south than they are in the north (see, for example, geological maps of Zen (1961) and Rowley et al. (1979)).

Graptolites

Strain values have been determined for the SR sites using three techniques: thecal spacing of graptolites, strain fringes around subspherical core objects, and reconstruction of pyrite blocks composing the graptolites. Direct comparison of the strain fringe and graptolite results can be made only along directions that S_0 and S_2 have in common, i.e., in the S_0/S_2 plane at site SR1 and along the S_0-S_2 intersection lineation at sites SR3 and SR5. For site SR1, the graptolite thecal spacing analysis yields values for $1 + e_1$ and $1 + e_2$ of 1.24 and 0.57, respectively (Goldstein et al., 1998). The strain fringes, in contrast, yield values for $1 + e_1$ and $1 + e_2$ of 1.65 and 1.3, respectively. The values obtained from the two approaches not only do not agree, but, for the *Y*-axis, the thecal spacing measurements indicate shortening, whereas the strain fringes indicate extension. The value for $1 + e$ along the S_0-S_2 intersection lineation determined from graptolite thecal spacing for sites SR3 and SR5 is 0.97 in both cases (Goldstein et al., 1998). The strain fringes give higher values for $1 + e$ along the S_0-S_2 intersection lineation for sites SR3 and SR5 of 1.15 and 1.30, respectively.

Although the thecal spacing of the graptolites and the strain fringes record different amounts of strain, the microstructure of the graptolites agrees with the strain fringes. At site SR1, the pyrite forming the graptolites has undergone chocolate tablet boudinage. This is consistent with the radial character of the strain fringes. Thus, shortening is indicated for the *Y*-axis by the graptolite thecal spacing, and extension is indicated for the *Y*-axis by the graptolite microstructure and strain fringes.

Comparison of strain values obtained from the strain fringes with those obtained from reconstruction of the pyrite blocks composing the graptolites shows that the strain fringes record more extension than the displaced pyrite blocks. As noted above, average values for $1 + e_1$ and $1 + e_2$ determined from the strain fringes for site SR1 are 1.65 and 1.3, respectively, whereas preliminary values for $1 + e_1$ and $1 + e_2$ determined from pyrite block reconstructions for site SR1 are 1.35 and 1.2, respectively. In addition, as noted above, average values for $1 + e$ along the S_0-S_2 intersection lineation for SR5 determined from the strain fringes and from the pyrite block reconstructions are 1.3 and 1.15, respectively.

The discrepancies in strain values suggest that the various strain markers record different portions of the total strain undergone by the strata. The spacing of the graptolite thecae is affected by any deformational event that occurred after deposition of the graptolite-bearing strata and changed length in the S_0 plane. The displaced pyrite blocks, in contrast, record the deformation that occurred after pyritization of the graptolites. The strain fringes, as noted above, record the strain related to S_2 development. The strain values obtained using graptolite thecal spacing, therefore, imply that the strata underwent shortening parallel to the *Y*-axis prior to the formation of the strain fringes and the pyritization of the graptolites. Subsequent extension was not sufficient to recover the shortening undergone by the strata during this early event, resulting in net shortening of the graptolites along the *Y*-axis. The strain values obtained by reconstruction of the pyrite blocks composing the graptolites, which are consistently lower than those obtained from the strain fringes, imply that pyritization of the graptolites occurred during low-grade metamorphism accompanying S_2 development.

The F_2 folds in the Taconic slate belt are interpreted as flexural folds (Crespi and Byrne, 1987). In theory, flexural folding does not result in changes in length in the S_0 plane, which acts as the shear plane during rotation of the fold limbs. In the absence of direct evidence pointing toward deformation in the S_0 plane during folding, a deformational event other than folding is sought as the cause of early shortening of the strata along the *Y*-axis. Pre-F_2 layer-parallel shortening is a candidate. Unfolding of S_0 at site SR1, which lies on the overturned limb of the fold, rotates the *Y*-axis from north-northeast trending to northwest trending (Fig. 7). This is consistent with the inferred convergence direction during Taconian orogenesis and supports the possibility that the strata underwent layer-parallel shortening during initial incorporation into the Taconic accretionary wedge.

The Mount Merino Formation directly underlies the Pawlet Formation (Fig. 2), which is correlative with the Austin Glen Graywacke and widely accepted to be Taconic flysch. Although many workers (Zen, 1961, 1964, 1967; Shumaker, 1967; Steuer and Platt, 1981; Platt and Steuer, 1982) have inferred an angular unconformity at the base of the Pawlet Formation, Rowley et al. (1979) and Bosworth et al. (1982) concluded that the Pawlet Formation conformably overlies the Mount Merino Formation and that stratigraphic omission between the Pawlet Formation and underlying units in the Taconic sequence, in most cases, is structural. Regardless, the Mount Merino and Pawlet formations contain graptolite fauna belonging to the same zone (Berry, 1962), implying that deposition of the Mount Merino Formation occurred shortly before the formation of synorogenic deposits.

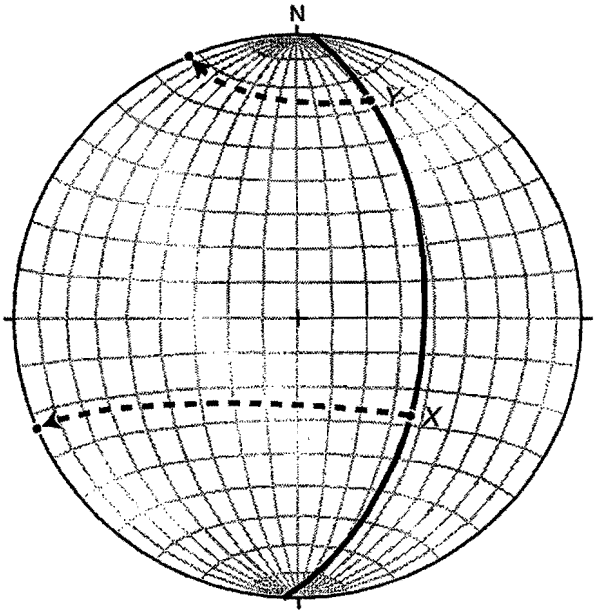

Figure 7. Stereoplot showing rotation of S0/S2 and *X*- and *Y*-axes to horizontal for site SR1. Equal-area, lower-hemisphere projection.

The preceding suggests that the Mount Merino Formation was only partially lithified when it was incorporated into the Taconic accretionary wedge. The proposed early layer-parallel shortening, therefore, may have resulted in tectonic consolidation of the strata such that the volume loss calculated from graptolite thecal spacing reflects, at least in part, loss of porosity rather than rock mass. A minimum value for the amount of shortening related to early layer-parallel shortening can be obtained using data from site SR1 by removing the strain recorded by the strain fringes from that recorded by the graptolite thecal spacing along the *Y*-axis. This results in approximately 55% shortening.

Strain values determined from reconstruction of the pyrite blocks composing the graptolites can be used to estimate the volume change during S_2 development, because pyritization of the graptolites is inferred to have occurred during S_2 development. Minimum and maximum values for the volume change are calculated as a result of cut-effect problems in strain estimation, as discussed above. Minimum and maximum estimates using the preliminary values for $1 + e_1$, $1 + e_2$, and $1 + e_3$ are 0% volume change and 30% volume gain. Because the cut-effect problems result in overestimation of the stretch, we suspect that the minimum volume change estimate is closer to the actual volume change undergone by the strata during S_2 development. These data, therefore, point to approximately constant-volume deformation during S_2 development. Note that the results do not depend on $1 + e_3$ values calculated from the hinge zone of the fold and that the results support the possibility of minor volume gain in fold limbs (see interpretation of reduction spots below).

Geometric relations at site SR3 permit an alternative approach to the understanding of volume change during S_2 development. Graptolites at this site show evidence of imbrication and boudinage, indicating that they have rotated from the instantaneous shortening field into the instantaneous extension field. The following analysis (Fig. 8) describes geometries viewing to the northeast. In the *XZ* plane, the graptolites lie 39° counterclockwise from S_2.

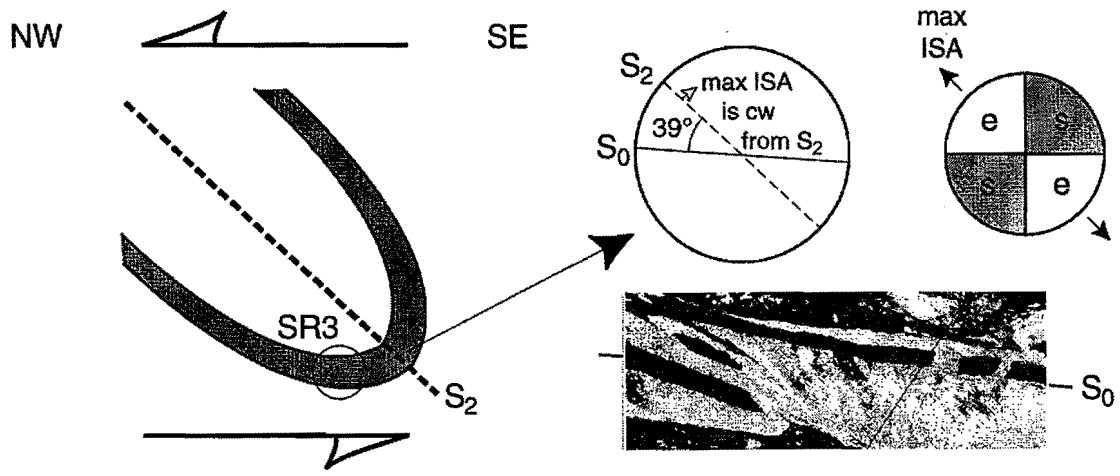

Figure 8. Schematic diagram of S0-S2 relations at site SR3 drawn for *XZ* plane. Graptolites in S0 show evidence of imbrication and boudinage, indicating that they have rotated from instantaneous shortening field into instantaneous extension field. Geometry implies angle between maximum instantaneous stretching axis (max ISA) and line separating extension and shortening fields is at least 39°. Instantaneous strain ellipse on far right shows extension (e) and shortening (s) fields for plane-strain, constant-volume deformation. Instantaneous strain ellipse is not oriented with respect to geographic reference frame. Note geometry, i.e., presence of graptolites that have undergone shortening and extension at an acute angle counterclockwise from S2, is inconsistent with simple shearing (see, for example, Ramsay (1967) and Passchier and Trouw (1996)). Photomicrograph is approximately 350 microns long. Plane polarized light. See text for discussion.

Because the sense of shear is top-to-northwest, S_2 rotated counterclockwise with respect to the shear plane as S_2-related strain accumulated. For plane-strain, constant-volume deformation, the lines of no infinitesimal strain lie at 45° to the maximum instantaneous stretching axis. The maximum instantaneous stretching axis lies clockwise from S_2, because of the counterclockwise rotation of S_2 during strain accumulation, i.e., S_2 initiated parallel to the maximum instantaneous stretching axis. Therefore, the angle between the graptolites and the maximum instantaneous stretching axis in the *XZ* plane is at least 39°. Given that S_2 has rotated to some extent and that the graptolites have rotated past the line of no infinitesimal strain, these geometric relations are consistent with constant-volume deformation. They are also consistent with volume-gain deformation (see, for example, Fig. 7 of Passchier (1990)). We are currently extending the analysis to include flattening strain in order to determine the extent to which the geometric relations preclude volume-loss deformation.

Reduction Spots

In using the reduction spot data to infer a deformation path, Goldstein et al. (1995) noted that there is no clear difference between the shape of the strain ellipsoid for limb sites and hinge sites. This is the case only if the sites are viewed as a whole. Because the strain fringe and S_2 data imply relatively low structural levels to the north and relatively high structural levels to the south, the reduction spot data (Fig. 6) can be divided into two domains. Sites SH and CP, which are located north of the transect studied by Chan (1998), are inferred to lie at a relatively low structural level, and sites QA through QF, which are located south of the transect studied by Chan (1998) and north of the SR sites, are inferred to lie at an intermediate structural level. When grouped by domain, there is a distinction between limb sites and hinge sites such that *YZ* axial ratios are greater for hinge as opposed to limb sites. In addition, *YZ* axial ratios, overall, are higher for the SH/CP domain than for the QA-QF domain, which is consistent with the structural level interpretation. These observations suggest that inference of a deformation path requires separation of the data by domain.

If the reduction spot data are grouped by domain and weighted means are used, then approximately 15% volume loss is required to derive the strain ellipsoid for the hinge site CP from that for the limb site SH and approximately 35% volume loss is required to derive the strain ellipsoid for the hinge site QD from that for the limb sites QA-QC/QF (50% from QA and 30% from the mean of the other three). These values are lower than the 55% volume loss calculated by Goldstein et al. (1995). Unlike Goldstein et al. (1995), who proposed that the 55% volume loss is a minimum estimate for the volume loss undergone by the strata during S_2 development, we propose that the calculated 15% to 35% volume loss is the total amount of volume loss undergone during S_2 development and applies only to hinge zone strata. This interpretation is based on absolute changes in length recorded by strain fringes around pyrite framboids in black slate of the Taconic sequence. The strain fringes show that the strata were undergoing extension along the *X*-axis during S_2 development and that the amount of extension along the *X*-axis was relatively uniform at a given structural level. Thus, if the strata are, for example, undergoing plane-strain deformation, then the *XY* axial ratio of the reduction spots will increase during S_2 development and the increase will be the same across a fold. The greater *YZ* axial ratio for hinge as opposed to limb sites results from greater shortening along the *Z*-axis at the hinge sites. We note that calculaton of the volume loss values given above assumes constant-volume deformation for the limb sites. The data are also consistent with regional-scale, constant-volume deformation, if fold limbs underwent volume gain, in which case less volume loss is required for fold hinges.

On the basis of geochemical data, Erslev (1998) concluded that the Mettawee Formation did not undergo large nonvolatile volume loss during S_2 development. He used two lines of evidence. First, compositional data for the Taconic slate belt, most of which is from samples of the Mettawee Formation, show that the SiO_2/Al_2O_3 and SiO_2/TiO_2 ratios of the slates, on average, are higher than those of Paleozoic shales (see Fig. 10 of Erslev (1998)). This pattern does not indicate large volume loss during S_2 development, unless the protolith of the Mettawee Formation was anomalously high in silica. And second, samples of Mettawee Formation from the Cedar Point quarry have low Zr (see Fig. 12 of Erslev (1998)), which is not consistent with enrichment in this relatively immobile element during S_2 development.

Our interpretation of the reduction spot data is broadly consistent with Erslev's (1998) inference of minimal nonvolatile volume loss during S_2 development. Although we suggest volume loss during S_2 development for the Mettawee Formation, the amount of volume loss is relatively low and occurs only in the hinge zones of the F_2 folds. Hinge zones in the Taconic slate belt are tight, and so most of the strata occupy limb positions. We also note that geochemical data suggest that large element fluxes can occur between the hinge and limbs of a fold or between the inner and outer arcs of a fold, in some cases the hinge or inner arc undergoing volume gain and in other cases volume loss (Gratier, 1983; Erslev, 1998). These data, however, are for mesoscale folds rather than regional-scale folds. Erslev (1998) analyzed samples from the same stratigraphic horizon around the fold hinge exposed in the Cedar Point quarry and noted uniform SiO_2/TiO_2 and Al_2O_3/TiO_2 ratios for samples described as being from the hinge and from the limb. He inferred no significant flux of silicate components. Because the Cedar Mountain syncline is a regional-scale fold, the samples from the quarry are all effectively in the hinge zone of the fold and so large fluxes would not be expected. Although it may not be statistically significant, the quarry samples show a slight overall decrease in SiO_2/TiO_2 in the hinge compared to the limb (see Fig. 11 of Erslev (1998)), which is consistent with the proposal of localization of volume loss in fold hinge zones.

THE BIRD MOUNTAIN FAULT: PREVIOUS AND CURRENT WORK

The Bird Mountain fault is a west-directed, low-angle thrust that bounds the Bird Mountain slice (Fig. 3). The fault is well exposed along and near the eastern shore of Lake St. Catherine in Wells, Vermont, and along Route 30 south of Wells. Excellent exposures within the fault zone provide evidence for its movement history in the context of the tectonic evolution of the Taconic Allochthon. Previous structural interpretations have addressed the Bird Mountain slice in a regional context, focusing in particular on the stacking order of the various Taconic slices and the relative timing of their emplacement. We review past research related to the Bird Mountain slice and present a detailed description of structural features observed within the Bird Mountain slice and Bird Mountain fault zone. The

meso- and microscale structural features support a synkinematic relation between thrusting along the Bird Mountain fault and the development of S_2.

Zen (1961) mapped the Bird Mountain slice as a recumbently folded, west-directed klippe. The slice lies structurally above the Giddings Brook slice, a slice of similar stratigraphy and structural style. Since Zen (1961), opposing interpretations of slice stacking order, timing of S_2 development relative to slice emplacements, and general tectonic interpretations of the Taconic Allochthon have been proposed by subsequent researchers.

Zen (1967) was the first to propose a west-to-east stacking order such that higher slices to the east were emplaced after an initial gravity-slide emplacement of the Giddings Brook and Sunset Lake slices. In addition, Zen (1967) described the nature of the contact between the Bird Mountain and Giddings Brook slices as a sharp, low-angle fault. The Edgerton half-window within the Bird Mountain slice exposes the Giddings Brook slice and controls the topographic expression of the Bird Mountain fault. Shumaker (1967) mapped the southern Bird Mountain slice within the Pawlet quadrangle and described a slice emplacement history similar to Zen (1967).

Further developing his slice theory, Zen (1972) modified his previous implicit interpretation that S_2 formed during the emplacement of the Giddings Brook slice. Evidence from mapping in the higher slices (Zen and Ratcliffe, 1971) indicated that F_2 folding accompanied or immediately followed emplacement of the highest slice. Development of S_2, therefore, was inferred to postdate emplacement of the Giddings Brook slice on the basis of the west-to-east stacking order and axial planar character of S_2 to the F_2 folds. Implicit in this interpretation is the assumption that S_2 developed simultaneously throughout the Taconic Allochthon. Zen (1972) speculated that S_2 developed as the higher slices were emplaced above the Giddings Brook slice but concluded that S_2 probably postdated emplacement of the Allochthon.

In contrast to Zen's interpretations, Rowley et al. (1979) and Rowley and Kidd (1981) proposed an east-to-west stacking order on the basis of the stratigraphic position of the flysch within individual thrust slices and modern subduction/accretionary wedge analogs. They described faults in the Giddings Brook slice as syn to late D_2/S_2, noting that the cleavage within the fault zones is parallel to subparallel to the regional S_2 cleavage (Rowley et al., 1979) (Rowley et al. (1979) define S_1 to be the regional slaty cleavage here defined as S_2). Bosworth and Rowley (1984) maintained the east-to-west stacking order but reinterpreted the D_2 faults of Rowley et al. (1979) as D_3 faults.

Stanley and Ratcliffe (1985) supported Zen's interpretation. They argued that the emplacement of the Bird Mountain slice predated S_2 and associated metamorphism on the basis of the observation that S_2 cuts across the Bird Mountain slice. Goldstein et al. (1995) also supported the view that thrusting predated S_2, noting that S_2 cuts across the Bird Mountain fault without changing orientation. Because the fault truncates F_2 folds, they inferred a sequence of events described by F_2 folding, followed by thrusting, followed by S_2 development. Most recently, Ratcliffe (1999) correlated the Bird Mountain slice with the Chatham slice to the south and maintained the view that the emplacement of younger slices was eastward toward the hinterland.

Metamorphism of the Taconic Allochthon may have been time transgressive (Karabinos, 1988). This has implications for interpretations that consider the formation of S_2 across different slices of the Allochthon to be a single event. S_2 may have formed at different times spatially and so is potentially not a reliable time marker. Another approach to understanding the structural relations within the Taconic Allochthon is to examine meso- and microscale structural features within the slice-boundary faults and the relations of these features to the different cleavages.

New observations suggest that movement along the Bird Mountain fault was coeval with the S_2 cleavage event. Abundant boudined quartz veins form a network, parallel and subparallel to S_2, and are concentrated along the thrust. The veins have been observed at the outcrop, hand-sample, and thin-section scales (Fig. 9). Locally, fibrous quartz within the veins is parallel to S_2. Fragments of slate with a well-developed S_2 are rotated within the fibrous quartz matrix. In addition, chlorite inclusion bands fringe the fragments of slate. The chlorite forms bands parallel to the fragment walls and interfingers with the fibrous quartz. The veins are interpreted to be associated with thrusting along the Bird Mountain fault, because they are spatially associated with the fault. The boudins imply that the veins

formed before or at the same time as S_2. The fragmented and rotated slate suggests that the veins postdated S_2. The chlorite inclusion bands suggest a crack-seal mechanism (Ramsay, 1980; Cox and Etheridge, 1983) that operated during or post S_2. These observations indicate an intimate relation between S_2 and vein formation: the veining is not exclusively pre-S_2 and not exclusively post-S_2, and so is interpreted as syn-S_2.

D_3 structures are also present within the Bird Mountain slice. S_3, which is typically a crenulation cleavage but may also be a disjunctive cleavage, is observed within the slice. These structures strike north-northeast and dip steeply to the east, and are parallel to the regional D_3 structures mapped by Chan (1998) to the north along Route 4. Parallel to the crenulations are asymmetric chevron folds of meter to centimeter scale that intensify close to the fault zone. These chevron folds are observed in outcrops along the topographic expression of the fault and within the interior of the slice. Similar D_3 structures were observed by Rowley et al. (1979) to the west of the Bird Mountain fault. Figure 10 shows the D_2 and D_3 structures recorded within the Bird Mountain slice.

The outcrops along the Bird Mountain fault near and south of Wells, Vermont, are interpreted to be within a pressure-solution shear zone, in which S_2 cleavage formation and large-scale thrust faulting occurred simultaneously. The fault zone is at least several hundred meters thick and contains both ductile and brittle deformational structures at a variety of scales. Preliminary observations at outcrop, hand-sample, and thin-section scales indicate that the Bird Mountain fault was active during S_2 development. Reactivation of the fault may have occurred during the D_3 event considering the spatial pattern of chevron folds within and near the fault zone, but this relation is not clear.

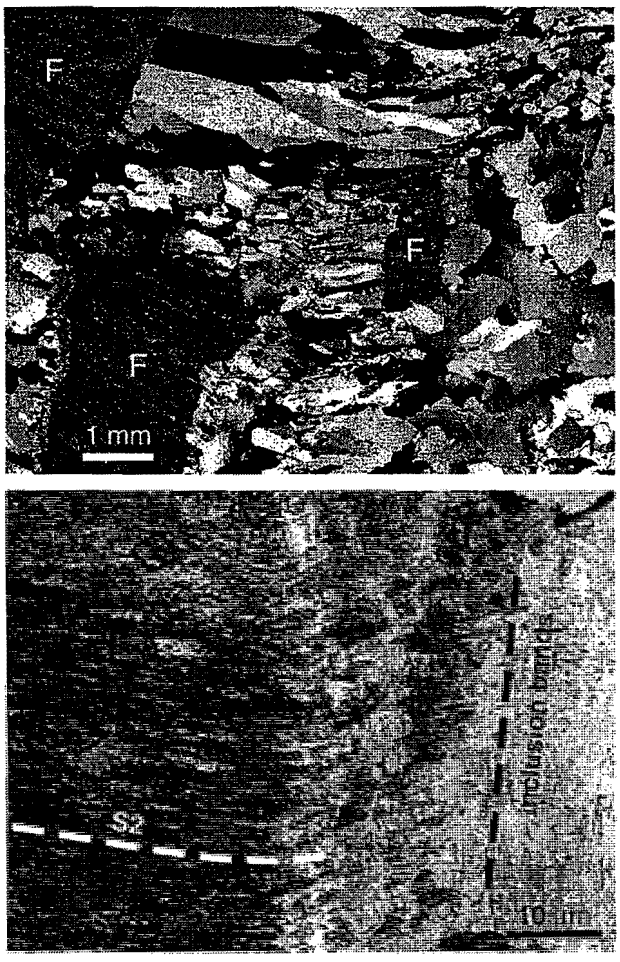

Figure 9. Photomicrographs of (top) rotated slate fragments (F) in a matrix of fibrous quartz that grew parallel to S2 (crossed polarized light) and (bottom) chlorite inclusion bands within S2-parallel fibrous quartz (plane polarized light).

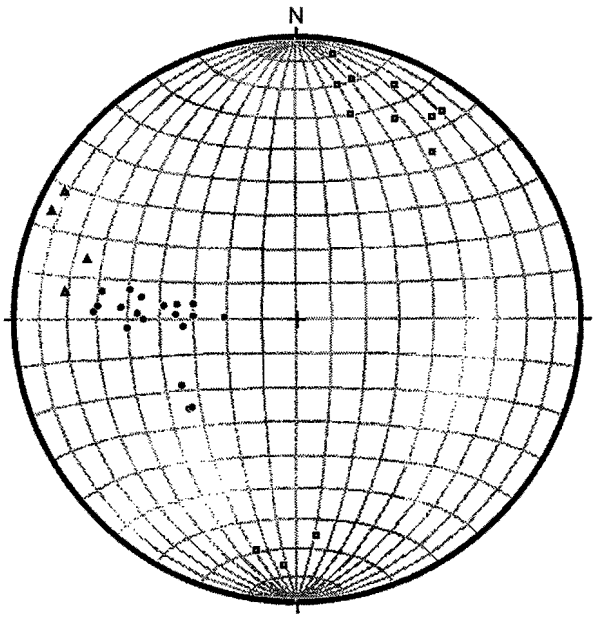

Figure 10. Stereoplot of structural elements associated with Bird Mountain fault. Solid circles represent poles to S2. Triangles represent poles to S3. Boxes represent F3 fold axes. Equal-area, lower-hemisphere projection.

ACKNOWLEDGEMENTS

JMC thanks her GEOL 217 students, who, over the years, have helped guide her understanding of the structural development of the Taconic orogenic belt. JMC and JRG thank Art Goldstein for helpful discussions on the Bird Mountain fault and Taconic geology in general.

REFERENCES CITED

Ando, C.J., Czuchra, B.L., Klemperer, S.L., Brown, L.D., Cheadle, M.J., Cook, F.A., Oliver, J.E., Kaufman, S., Walsh, T., Thompson, J.B., Jr., Lyons, J.B., and Rosenfeld, J.L., 1984, Crustal profile of mountain belt: COCORP deep seismic-reflection profiling in New England Appalachians and implications for architecture of convergent mountain chains: American Association of Petroleum Geologists Bulletin, v. 68, p. 819-837.

Berry, W.B.N., 1962, Stratigraphy, zonation, and age of Schaghticoke. Deepkill, and Normanskill shales, eastern New York: Geological Society of America Bulletin, v. 73, p. 695-718.

Bosworth, W., and Rowley, D.B., 1984, Early obduction-related deformation features of the Taconic Allochthon: Analogy with structures observed in modern trench environments: Geological Society of America Bulletin, v. 95, p. 559-567.

Bosworth, W., Rowley, D.B., and Kidd, W.S.F., 1982, A structure section in eastern New York showing variation in style of deformation across the Taconic Allochthon: Discussion: Northeastern Geology, v. 4, p. 111-116.

Chan, Y.C., 1998, Kinematic and geochronologic constraints on the structural development of the northern Taconic Allochthon in western New England, USA [Ph.D. thesis]: Storrs, University of Connecticut, 117 p.

Chan, Y.C., Crespi, J.M., and Hodges, K.V., 2001, Dating cleavage formation in slates and phyllites with the $^{40}Ar/^{39}Ar$ laser microprobe: An example from the western New England Appalachians, USA: Terra Nova, v. 12, p. 264-271.

Chapple, W.M., 1973, Taconic orogeny: Abortive subduction of the North American continental plate?: Geological Society of America Abstracts with Programs, v. 5, p. 573.

Cox, S.F., and Etheridge, M.A., 1983, Crack-seal fiber growth mechanisms and their significance in the development of oriented layer silicate microstructures: Tectonophysics, v. 92, p. 147-170.

Crespi, J.M., and Byrne, T., 1987, Strain partitioning and fold kinematics in the Giddings Brook slice, Taconic Allochthon, west-central Vermont: Geological Society of America Abstracts with Programs, v. 19, p. 9.

Crespi, J.M., and Chan, Y.C., 1996, Vein reactivation and complex vein intersection geometries in the Taconic slate belt: Journal of Structural Geology, v. 18, p. 933-939.

Dale, T.N., 1899, The slate belt of eastern New York and western Vermont: U. S. Geological Survey, 19th Annual Report, pt. 3, p. 153-300.

Durney, D.W., and Ramsay, J.G., 1973, Incremental strains measured by syntectonic crystal growths, *in* De Jong, K.A., and Scholten, R., eds., Gravity and Tectonics: New York, Wiley, p. 67-96.

Erslev, E.A., 1998, Limited, localized nonvolatile element flux and volume change in Appalachian slates: Geological Society of America Bulletin, v. 110, p. 900-915.

Goldstein, A., Knight, J., and Kimball, K., 1998, Deformed graptolites, finite strain and volume loss during cleavage formation in rocks of the Taconic slate belt, New York and Vermont, USA: Journal of Structural Geology, v. 20, p. 1769-1782.

Goldstein, A., Chan, Y.C., Pickens, J., and Crespi, J.M., 1997, Deformation of the Taconic sequence, western Vermont and eastern New York, *in* Grover, T.W., Mango, H.N., and Hasenohr, E.J., eds., New England Intercollegiate Geological Conference Guidebook: Castleton, Vermont, Castleton State College, p. A1-1:31.

Goldstein, A., Pickens, J., Klepeis, K., and Linn, F., 1995, Finite strain heterogeneity and volume loss in slates of the Taconic Allochthon, Vermont, USA: Journal of Structural Geology, v. 17, p. 1207-1216.

Gratier, J.P., 1983, Estimation of volume changes by comparative chemical analyses in heterogeneously deformed rocks (folds with mass transfer): Journal of Structural Geology, v. 5, p. 329-339.

Hoak, T.E., 1992, Strain analysis, slaty cleavage and thrusting in the Taconic slate belt, west-central Vermont: Northeastern Geology, v. 14, p. 7-14.

Karabinos, P., 1988, Heat transfer and fault geometry in the Taconian thrust belt, western New England, *in* Mitra, G., and Wojtal, S., eds., Geometries and Mechanisms of Thrusting, With Special Reference to the Appalachians: Geological Society of America Special Paper 222, p. 35-45.

Karabinos, P., Samson, S.D., Hepburn, J.C., and Stoll, H.M., 1998, Taconian orogeny in the New England Appalachians: Collision between Laurentia and the Shelburne Falls arc: Geology, v. 26, p. 215-218.

Karabinos, P., Samson, S.D., Hepburn, J.C., and Stoll, H.M., 1999, Taconian orogeny in the New England Appalachians: Collision between Laurentia and the Shelburne Falls arc: Reply: Geology, v. 27, p. 382.

Laird, J., Lanphere, M.A., and Albee, A.L., 1984, Distribution of Ordovician and Devonian metamorphism in mafic and pelitic schists from northern Vermont: American Journal of Science, v. 284, p. 376-413.

Passchier, C.W., 1990, Reconstruction of deformation and flow parameters from deformed vein sets: Tectonophysics, v. 180, p. 185-199.

Passchier, C.W., and Trouw, R.A.J., 1996, Microtectonics: Berlin, Springer-Verlag, 289 p.

Passchier, C.W., and Urai, J.L., 1988, Vorticity and strain analysis using Mohr diagrams: Journal of Structural Geology, v. 10, p. 755-763.

Platt, L.B., and Steuer, M.R., 1982, A structure section in eastern New York showing variation in style of deformation across the Taconic Allochthon: Reply: Northeastern Geology, v. 4, p. 117-119.

Ramsay, J.G., 1967, Folding and fracturing of rocks: New York, McGraw-Hill, 568 p.

Ramsay, J.G., 1980, The crack-seal mechanism of rock deformation: Nature, v. 284, p. 135-139.

Ramsay, J.G., and Graham, R.H., 1970, Strain variation in shear belts: Canadian Journal of Earth Sciences, v. 7, p. 786-813.

Ratcliffe, N.M., 1999, Examination of the slice concept and evidence for primary emplacement structures in the Taconic Allochthons of western New England: Geological Society of America Abstracts with Programs, v. 31, p. 62.

Ratcliffe, N.M., Hames, W.E., and Stanley, R.S., 1998, Interpretation of ages of arc magmatism, metamorphism, and collisional tectonics in the Taconian orogen of western New England: American Journal of Science, v. 298, p. 791-797.

Ratcliffe, N., Hames, W.E., and Stanley, R.S., 1999, Taconian orogeny in the New England Appalachians: Collision between Laurentia and the Shelburne Falls arc: Comment: Geology, v. 27, p. 381.

Rowley, D.B., and Kidd, W.S.F., 1981, Stratigraphic relationships and detrital composition of the medial Ordovician flysch of western New England: Implications for the tectonic evolution of the Taconic orogeny: Journal of Geology, v. 89, p. 199-218.

Rowley, D.B., Kidd, W.S.F., and Delano, L.L., 1979, Detailed stratigraphic and structural features of the Giddings Brook slice of the Taconic Allochthon in the Granville area, *in* Friedman, G.M., ed., New York State Geological Association and New England Intercollegiate Geological Conference Guidebook: Troy, New York, Rensselaer Polytechnic Institute, p. 186-242.

Sanderson, D.J., 1982, Models of strain variation in nappes and thrust sheets: A review: Tectonophysics, v. 88, p. 201-233.

Shumaker, R.C., 1967, Bedrock geology of the Pawlet quadrangle, Vermont: Part 1, central and western portions: Vermont Geological Survey Bulletin, no. 30, p. 1-59.

Stanley, R.S., and Ratcliffe, N.M., 1985, Tectonic synthesis of the Taconian orogeny in western New England: Geological Society of America Bulletin, v. 96, p. 1227-1250.

Steuer, M.R., and Platt, L.B., 1981, A structure section in eastern New York showing variation in style of deformation across the Taconic Allochthon: Northeastern Geology, v. 3, p. 134-137.

Sutter, J.F., Ratcliffe, N.M., and Mukasa, S.H., 1985, $^{40}Ar/^{39}Ar$ and K-Ar data bearing on the metamorphic and tectonic history of western New England: Geological Society of America Bulletin, v. 96, p. 123-136.

Weijermars, R., 1991, The role of stress in ductile deformation: Journal of Structural Geology, v. 13, p. 1061-1078.

Wood, D.S., 1974, Current views of the development of slaty cleavage: Annual Review of Earth and Planetary Sciences, v. 2, p. 369-401.

Zen, E-an, 1961, Stratigraphy and structure at the north end of the Taconic Range in west-central Vermont: Geological Society of America Bulletin, v. 72, p. 293-338.

Zen, E-an, 1964, Stratigraphy and structure of a portion of the Castleton quadrangle, Vermont: Vermont Geological Survey Bulletin, no. 25, 70 p.

Zen, E-an, 1967, Time and space relationships of the Taconic Allochthon and Autochthon: Geological Society of America Special Paper 97, 107 p.

Zen, E-an, 1972, Some revisions in the interpretation of the Taconic Allochthon in west-central Vermont: Geological Society of America Bulletin, v. 83, p. 2573-2587.

Zen, E-an, and Ratcliffe, N.M., 1971, Bedrock geologic map of the Egremont quadrangle and adjacent areas, Berkshire County, Massachusetts and Columbia County, New York: U.S. Geol. Survey Misc. Invest. Map, I-628, 4 p.

ROAD LOG

Mileage

0.0 Trip will begin in Fort William Henry Conference Center parking lot.
3.5 Turn left onto Route 149 east.
15.1 Turn left at light in Fort Anne onto Route 4 north.
25.5 At Whitehall turn right, continuing on Route 4 north (see Fig. 11 for trip route).
30.0 STOP 1. Turn left into driveway just before billboards on hill to left and park in overgrown lot.

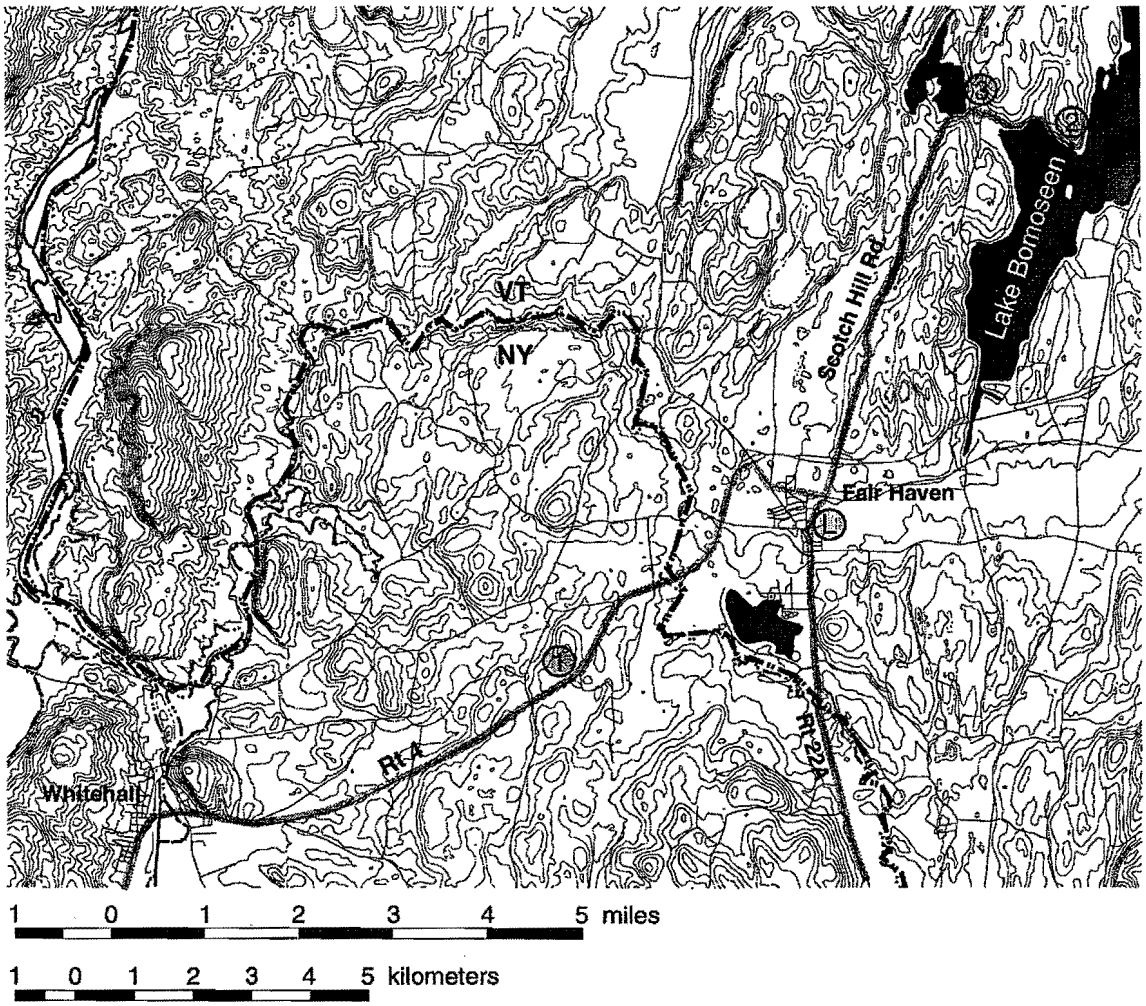

Figure 11. Location map for northern part of field trip. Highlighted roads indicate trip route. Numbered circles indicate stop localities; circled L is lunch stop.

STOP 1. ABANDONED QUARRY. (45 MINUTES) This quarry, which exposes the Cambrian Hatch Hill Formation, lies on the upright limb of the Mount Hamilton syncline, a regional-scale, west-vergent F_2 fold. S_0 lies at a low angle to S_2, which dips about 30°-35° to the east. Fibrous calcite veins are abundant in the strata and lie in a variety of orientations.

The outcrop was included by Chan (1998) in his transect of the Taconic slate belt in the vicinity of Route 4. Strain fringes around pyrite framboids in the strata record top-to-west-northwest, non-coaxial flow. Passchier and Urai (1988) used veins in the exposure to estimate the kinematic vorticity number of the flow. They inferred that the dominant vein set formed at some point during S_2 development; however, these veins and others display characteristics that suggest that they are early pre-folding veins, which were reactivated during S_2 development (Crespi and Chan, 1996). Determination of the flow type required estimation of volume change, which Passchier and Urai (1988) accomplished through geochemical analysis of a sample with a variably developed S_2. They determined a volume loss of 50%. Erslev (1998), in contrast, analyzed samples from the quarry with a penetrative S_2 and concluded, on the basis of geochemical data, that large volume loss occurred only at the scale of individual cleavage domains.

30.0 Turn left back onto Route 4 north.
31.9 Cross Vermont State line (Poultney River) and begin four-lane highway.
33.3 Take exit 2 off Route 4 (Fair Haven/Vergennes).
33.5 Take right off ramp onto Route 22A south.
33.8 Turn left onto Fourth Street.
34.4 Turn left at blinking red light onto Dutton Road (becomes Scotch Hill Road after crossing Route 4).
38.8 Scotch Hill syncline (Stop 3) on left. Bear right, staying on main paved road.
39.0 At Bomoseen State Park entrance take hard left onto Cedar Mountain Road (dirt road).
40.3 STOP 2. Cedar Point quarry. Road ends here. Park in pullout or on north side of road. Do not block driveway opposite quarry entrance. Refer to Fig. 12 for trail map of quarry.

STOP 2. CEDAR POINT QUARRY. (1 HOUR 15 MINUTES) The hinge zone of the Cedar Mountain syncline, a regional-scale, overturned, west-vergent, isoclinal F_2 fold, is exposed at this stop. The folded strata consist of the Cambrian Mettawee Formation. The dominant cleavage in the exposure is S_2, which dips about 25° to the east and is parallel to the axial plane of the fold. A moderately developed S_3 is also present.

Green ellipsoidal reduction spots are common in the maroon slate and can readily be seen in the abandoned blocks on the quarry floor. Irregularly shaped areas of reduction and bands of reduction subparallel to S_0 are also common. Measurements of the ellipsoidal reduction spots have been made by Wood (1974), Hoak (1992), and Goldstein et al. (1995). Minimum volume losses during S_2 development of 55% determined from the reduction spot data (Goldstein et al., 1995) are in conflict with geochemical data from the quarry, which are consistent with minimal nonvolatile volume loss (Erslev, 1998).

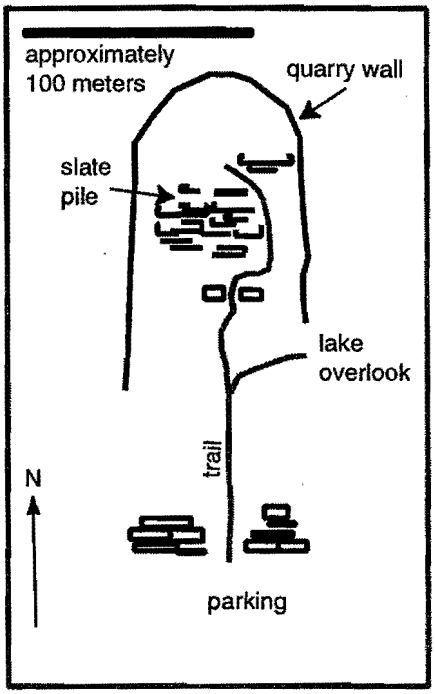

Figure 12. Trail map of Cedar Point quarry. Climb to top of slate pile from east side.

40.3 Return back along Cedar Mountain Road.
41.6 At Bomoseen State Park entrance take right onto Scotch Hill Road.
41.7 Bear left, staying on main paved road.
41.8 STOP 3. Scotch Hill syncline. Turn left into driveway of white house opposite syncline and park on grass to right of driveway. Additional parking on grass on either side of road.

STOP 3. SCOTCH HILL SYNCLINE. (45 MINUTES) This is a well known exposure in New England. The property owner asks that hammers not be used on the outcrop, so please leave your hammer in your vehicle. Also, poison ivy may be dense at the base of the exposure.

This exposure of the Ordovician Poultney Formation lies in the hinge zone of the Scotch Hill syncline, a regional-scale, west-vergent F_2 fold. S_2 dips about 30° to the east and is axial planar to the fold. En echelon, sigmoidal quartz veins provide evidence for flexural folding of the strata with pinning at the hinge. The veins are present on both limbs of the fold but are more systematic on the vertical limb and, thus, provide a better example of vein development within shear zones. (In this context, S_0 acts as the shear plane.) The veins are easily found on the vertical limb of the fold. To observe the veins on the gently dipping, upright limb, go around the small shed and climb to the base of the exposure behind the shed. Veins on both limbs of the fold are folded and/or boudined. On the vertical limb, the veins have a Z-shaped asymmetry (viewed to the north), indicating east-side-down sense of shear along S_0. On the gently dipping, upright limb of the fold, the veins have an S-shaped asymmetry (viewed to the north), indicating top-to-west sense of shear along S_0. Prefolding veins, which are not coaxial with the fold, can also be observed in the exposure. These appear approximately parallel to S_2 on the fold profile plane on both limbs of the fold, but three-dimensional exposures show that the veins lie at an angle to S_2. The prefolding veins lie in

approximately the same orientation on both limbs of the fold. This results because shearing within layering effectively cancelled the change in orientation from rigid rotation of the fold limbs.

41.8 Return back along Scotch Hill Road toward Fair Haven.
46.2 After crossing Route 4 go straight at blinking light to center of Fair Haven.
46.6 LUNCH STOP. Fair Haven green. Trip continues from here on Route 22A south to Middle Granville (see Fig. 13 for trip route).
58.5 Turn left off Route 22A and immediately cross bridge onto Washington County 24.
58.6 Turn left onto Depot Street (opposite Chapman's General Store).
59.3 Turn left onto Stoddard Road.
59.8 STOP 4. Stoddard Road graptolites. Park on right, opposite drained beaver pond under conversion to pasture.

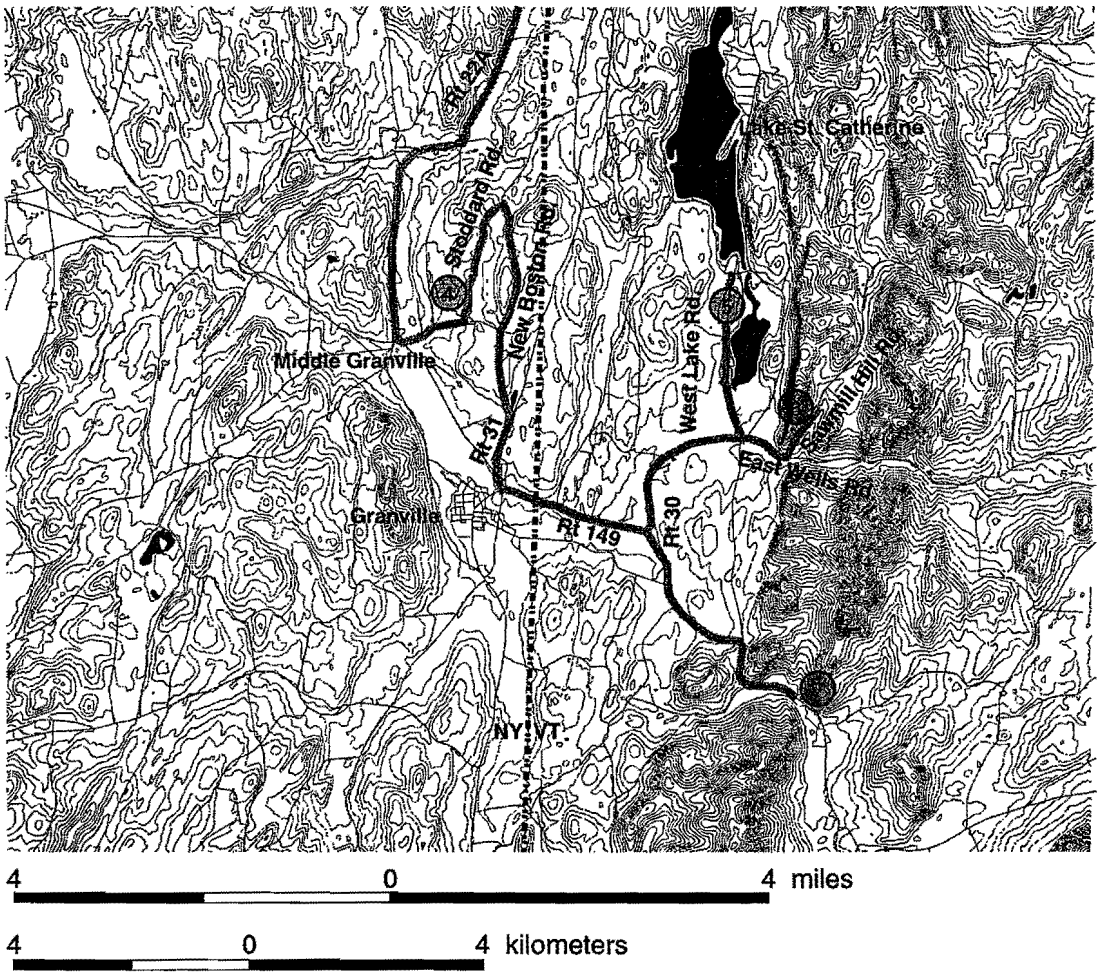

Figure 13. Location map for southern part of field trip. Highlighted roads indicate trip route. Numbered circles indicate stop localities.

STOP 4. STODDARD ROAD GRAPTOLITES. (1 HOUR) The first exposure (SR1) that we will visit at this stop is located immediately east of the road. The second exposure (SR2) is located on the small hill in the middle of the drained beaver pond and, if the area is marshy, can be reached by crossing the small stream at the south end of the drained pond. Both exposures are rather small. Please be kind to them with your hammers so that geologists on trips in the future can also enjoy the graptolites and structural features.

The two exposures are of the graptolite-bearing Stoddard Road Member of the Ordovician Mount Merino Formation. Exposures of the Mount Merino Formation in the vicinity of Stoddard Road are in the core of a regional-scale F_2 syncline. SR1 is located on the overturned limb of the syncline, and S_0 and S_2 are essentially parallel. S_0/S_2 dips about 45°-50° to the east. Graptolites are readily observed in place on the underside of the overhanging S_0/S_2 surfaces and in numerous pieces of float. The hinge zone of a mesoscale fold is exposed at the north end of the outcrop where graptolites can be observed on an S_0 surface at a very high angle to S_2. Mesoscale folds, which cannot be recognized using stratigraphic relations, may be common in the generally poorly exposed slates of the region. SR2 is located in the hinge zone of the regional-scale F_2 syncline. Well-preserved graptolites are present but more difficult to find at the exposure. S_0 lies at very high angles to S_2, which dips about 45°-50° to the east, and the exposure provides good examples of using S_0-S_2 relations to determine whether strata are on the upright or overturned limb of a fold. The axial-planar character of S_2 can be observed in the hinge of the fold, which is exposed on the north side of the hill in a small block that is probably slightly out of place.

59.8 Continue north on Stoddard Road.
60.8 Turn right onto New Boston Road.
62.3 Go straight at intersection with stop sign.
63.3 Turn right onto Route 25 south. Continue to center of Granville.
64.2 At Granville center turn left onto Route 149 east.
65.9 Turn left onto Route 30 north and continue to Wells.
66.7 Turn left onto North Street (Lakeside Realty) just before center green of Wells.
68.1 STOP 5. At top of grassy hill park on right.

STOP 5. BIRD MOUNTAIN FAULT OVERLOOK. (20 MINUTES) From this vantage point, the Bird Mountain fault is clearly expressed as the abrupt topographic transition between the valley containing Little Pond and Lake St. Catherine and the hills to the east. Good exposures of the fault can be viewed in a large roadcut along the east shore of Lake St. Catherine on Route 30, but access is limited and the orientation of the exposure is parallel to strike. To the east of the fault in this region, the Mettawee (St. Catharine Formation of Shumaker (1967)) and West Castleton/Hatch Hill formations underlie the hills of the Bird Mountain slice. Slate quarries are absent from the Bird Mountain slice despite the abundance of the Mettawee Formation. Zen (1967) noted that the Mettawee within the Bird Mountain slice is siltier than Mettawee to the west and, therefore, is unfit for roofing material.

68.1 Continue north on North Road.
68.4 At intersection with West Lake Road drive around traffic island and return past overlook.
70.1 Turn left onto Route 30 north.
70.2 At Wells green go straight onto East Wells Road as Route 30 turns to left.
70.4 Bear left up hill onto Sawmill Hill Road.
71.2 Stop 6. Park on right, opposite small roadcut.

STOP 6. BIRD MOUNTAIN SLICE. (45 MINUTES) This small outcrop records several deformational events to affect the Taconic Allochthon. The rocks are within the Mettawee Formation. S_0 is folded and the fold axes trend northwest. A variably spaced, axial planar S_2 cleavage cuts S_0. S_2 is well defined along limbs of folds but nearly absent in the hinges. A weak spaced cleavage, steeper than the pervasive S_2 cleavage, is interpreted to be S_3. Refer to Fig. 10 to see the local relation between S_2 and S_3. S_2-parallel veins are present at the south end of the outcrop.

71.2 Continue up Sawmill Hill Road to first driveway on left.
71.3 Turn around in driveway on left. Drive down Sawmill Hill Road.
72.1 Turn right onto East Wells Road.
72.3 At intersection go straight onto Route 30 south.
77.4 STOP 7. Turn into driveway of white house (3723 on mailbox). Park in driveway. Outcrop in backyard, northwest of house.

STOP 7. BIRD MOUNTAIN FAULT. (45 MINUTES) Outcrops in the yard behind the house, in the woods above, and along Route 30 (beware poison ivy!) contain abundant veins that are parallel and subparallel to S_2. This is the prominent S_2 cleavage that dominates the Allochthon from here west, but is folded in this manner only near the Bird Mountain fault. In addition, the S_2 surface and veins are deformed into asymmetric chevron folds. The green and purple rocks exposed here are the Mettawee Formation. The orientation of S_2 is highly variable due to the intense chevron folding.